DESIGN, FABRICATION, AND VALIDATION OF A TWO-DYE FLUORESCENCE PHANTOM FOR EXCITATION–EMISSION MATRIX HYPERSPECTRAL IMAGING BENCHMARKING

Fernando Villarruel[1], Narine Sarvazyan[1,2]

[1]L. A. Orbeli Institute of Physiology NAS RA, Yerevan, Armenia
[2]George Washington University, Washington, DC, United States

ABSTRACT

Excitation–emission matrix hyperspectral imaging (EEM-HSI) promises richer chemical discrimination than single- or multi-excitation hyperspectral imaging (3D-HSI and ME-HSI, respectively) by resolving a full excitation profile at every pixel. Benchmarking and validating unmixing algorithms for EEM-HSI requires a phantom with a known, spatially resolved ground truth in which the constituent fluorophores are chosen to stress the excitation dimension specifically. This paper describes the design, fabrication, and validation of a two-dye fluorescence phantom built from harmaline and harmine — a pair of structurally related β-carboline alkaloids whose emission bands overlap substantially while their excitation profiles remain distinguishable. We detail the rationale for this dye pair, the preparation of a seven-class mixture series spanning pure-dye endpoints to intermediate ratios, the protocol used to fix the mixtures in a spatially addressable array, and their usage in the EEM-HSI acquisition. The resulting phantom and its ground-truth mask are intended as a reusable benchmarking target for chemometric unmixing methods (e.g. MCR-ALS, PARAFAC) applied to EEM-HSI data.

Index Terms— fluorescence phantom, hyperspectral imaging, hyperspectral imaging calibration, excitation–emission matrix, harmaline, harmine, ground-truth dataset

1. INTRODUCTION

Multi-Excitation and Excitation–Emission Matrix Hyperspectral Imaging (ME-HSI and EEM-HSI, respectively) extend conventional single-excitation fluorescence (3D HSI) by acquiring image cubes across several excitation wavelengths (λ_{exc}). While 3D HSI captures emission spectra at a single λ_{exc} and ME-HSI collects emission data across a few discrete λ_{exc}, EEM-HSI measures a complete EEM at every pixel to resolve fluorophores with overlapping spectra. These approaches have attracted growing attention over recent years, seeing successful application in several domains – from biomedical fields to the analysis of biological samples and chemical compositions.[1], [2], [3], [4] However, demonstrating and benchmarking this capability requires a standard sample in which the ground-truth chemical composition is known at every pixel, and in which the constituent fluorophores are deliberately chosen so that emission wavelength (λ_{em}) dimension alone cannot separate them — otherwise the λ_{exc} dimension is never actually tested. Until now, published EEM-HSI and ME-HSI studies frequently use samples whose composition, preparation, and validation are reported only briefly, or not at all, which limits reproducibility and makes it difficult to compare unmixing algorithms across studies. The creation of a well-characterized phantom to test EEM-HSI acquisition and analysis methods addresses this need.

This paper documents the design and fabrication of a two-dye fluorescence phantom built specifically to test this "λ_{exc}-discriminating, λ_{em}-overlapping" regime, together with the steps used to validate that the phantom's actual composition matches its nominal design. One of the uses of the described phantom is to evaluate how illumination beam-shape deformation across excitation wavelengths distorts per-pixel excitation profiles recovered by EEM-HSI.

2. DYE SELECTION

A phantom intended to test λ_{exc}-based unmixing must be built from fluorophores that occupy a specific position in spectral-overlap space. Three regimes are possible for a two-component system: (*Scenario A*) the components differ in both λ_{exc} and λ_{em}, in which case even single-excitation imaging can separate them; (*Scenario B*) the components differ mainly in λ_{em}, with overlapping λ_{exc}, which conventional single- or ME-HSI handles via the λ_{em} dimension; and (*Scenario C*) the components differ mainly in λ_{exc}, with overlapping, unimodal emission bands — the case in which single-λ_{exc} 3D-HSI cannot separate the components, while multi-λ_{exc} HSI (ME-HSI) is misled into treating the mixture as a single fluorophore. In this latter case, only full EEM-HSI with per-pixel excitation resolution offers a route to unmixing. A benchmarking phantom should target *Scenario C* specifically, since it is the case that most directly exercises the added value EEM-HSI claims over ME-HSI and 3D-HSI.

Harmaline (Hlina) and harmine (Ha) were selected to instantiate *Scenario C*. Both are naturally occurring β-carboline alkaloids with closely related molecular structure

(Ha is the aromatic, fully unsaturated analogue; Hlina is the 3,4-dihydro derivative), which gives them fluorescence emission bands that overlap substantially and are both effectively unimodal, while their excitation behavior differs enough to be discriminable by a well-resolved excitation scan. Reference emission maxima in aqueous solution are approximately 417 nm for Ha and 486 nm for Hlina, [5] placing both well within the λ_{em} window (420–720 nm) and the λ_{exc} window (310–415 nm) used for the phantom imaging described below. Although the maximum λ_{exc} for the Ha will be truncated by the usage of a 425 nm long-pass filter coupled to the HSI camera (see *Section 3.3*), the resolution of the pair is expected to be possible with the available signal in the camera range.

Beyond their spectral suitability, Hlina and Ha were chosen for practical reasons:

1. Commercial availability at known purity, avoiding in-house synthesis or purification;
2. Sufficient fluorescence quantum yield and photostability across the tested excitation range to give usable signal at practical camera exposure times; [6], [7]
3. Hlina reported solubility is 1.07 g/L in phosphate buffer pH 7.4 at 310.15 K. For Ha, the only available experimental aqueous solubility data are reported at pH 7 (3.31×10^{-5} M ≈ 7.0 mg/L, 20°C); [8], [9]
4. It was previously shown that aqueous solutions of mixed Ha and Hlina can be resolved by chemometric analysis, obtaining each component concentration besides their spectral overlap.[6]

3. PHANTOM FABRICATION

3.1. Stock solutions and mixture series

Two ml of stock solutions of Hlina 2.54 µM and Ha 2.34 µM (*Aldrich*) were prepared in phosphate buffer (pH 7.4). Concentrations were determined by measuring the absorbance of each solution and considering the previously reported absorbance coefficients.[6] The chosen concentrations were selected to match the signal height of each dye at their respective $\lambda_{exc}/\lambda_{em}$ maxima, considering their absorption coefficients and fluorescence quantum yields. From those solutions, 200 µl of each Hlina/Ha mixture were prepared by combining the two stocks in the volumetric ratios summarized in **Fig 1**. Afterwards, the obtained solutions (pure dyes and mixtures) were diluted 50:50 with 10 % polyvinyl alcohol to a final 5% PVA concentration.

3.2. Phantom creation

To create the phantom, 5 µl aliquots of the above-mentioned mixtures (Hlina/Ha in phosphate/PVA 5%, aqueous solutions) were placed in a microscope slide to create a dot pattern (8.5 mm between one drop and the neighboring one) as the one depicted in **Fig 1**. Three repetitions of each solution were placed at different locations in the glass and were allowed to dry in the dark overnight. This protocol is intended to physically fix the mixtures on the microscope slide and to allow repeated, non-destructive imaging across multiple light sources and sessions. The final obtained phantom consists of a 3 x 8 (rows x columns) array of solid dots of approximately 3.5 mm diameter, with each region large enough to contain a well-populated pixel area for per-class averaging after registration to the ground-truth mask. Region boundaries were kept apart to avoid optical or diffusive cross-contamination between adjacent classes. The usage of PVA as solid matrix yielded transparent solid dots, which avoids non-linear inner filter effects from highly absorptive matrices.

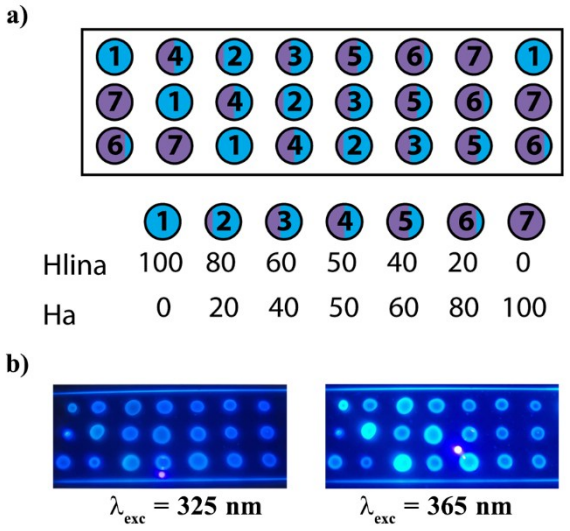


Fig. 1. (a) Schematic representation of the created phantom, exposing each dot position and their Hlina/Ha relative concentration. **(b)** Phantom photos under λ_{exc} = 325 nm and λ_{exc} = 365nm (left and right panel, respectively).

3.3. EEM-HSI data acquisition and correction

The prepared phantom was imaged using a HSI setup consisting of: (i) a multi-LED source (*WHeeLED, Mightex*; 310, 325, 340, 365, 385, 400, 415 nm, 10 nm FWHM) coupled to a liquid light guide (*Newport*) and a 425 nm short-pass filter (*Edmund Optics*); (ii) a NUANCE FX hyperspectral camera (*CRi*) coupled to a 425 nm long-pass filter (*Edmund Optics*), which acquires images in the 420 to 720 nm emission spectral range (10 nm step). Seven 3D HSI datasets were acquired under illumination with the above-mentioned λ_{exc}, without changing the geometry of the HSI

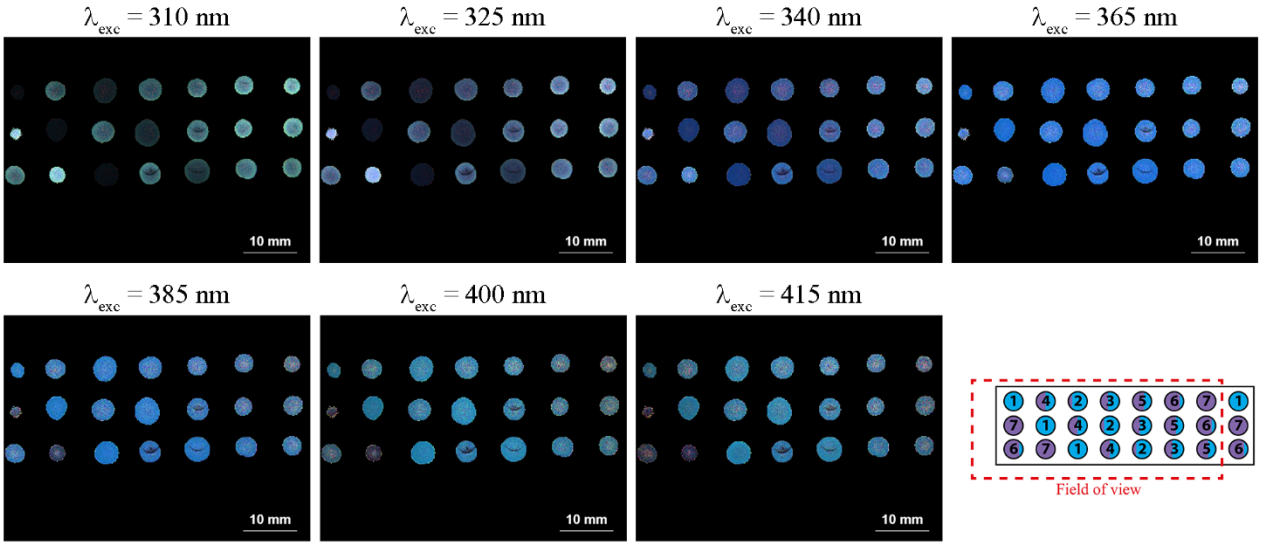


Figure 2. RGB representation of the HSI 3D cubes obtained at each different λ_{exc}. The scheme shows the HSI dataset field of view.

system. Then, the obtained data was re-arranged in a 4D-dataset with dimensions (x, y, λ_{exc}, λ_{em}), where each pixel has its own EEM. To maintain a perfectly balanced dataset of exactly three spatial replicates per class (3 * 7 array, 21 dots total), the redundant eighth column was excluded from the image acquisition to prevent class-imbalance bias during unmixing evaluation (**Fig 1(b)** and **Fig. 2**).

After the EEM-HSI data acquisition, the obtained data was corrected both by the lamp power at each λ_{exc} and the exposure time used in each 3D cube acquisition. Then, a min-max normalization was applied to each pixel, so every pixel's EEMs are in the 0-1 range of values. The RGB representations of the obtained HSI dataset, at each different λ_{exc}, are exposed in **Fig 2**.

3.4. Ground truth mask construction

The background pixels from the acquired HSI dataset were filtered by setting a signal threshold. A pixel-wise ground-truth mask was then manually constructed by registering the known array layout to the imaged field of view, assigning each pixel to one of the seven mixture classes or to background. This mask is intended to serve as a reference for any further instrumental or unmixing algorithms performance evaluation (e.g. Pearson correlation and R^2 of recovered vs. nominal Hlina fraction).

4. COMPOSITIONAL VALIDATION

From the obtained HSI dataset, the pure-dye endpoints (classes **(1)** 100:0 and **(7)** 0:100 Hlina:Ha relative concentration) serve as internal references: any unmixing algorithm applied to the full dataset should recover pure-component spectra qualitatively consistent with expected spectral behavior. This provides a data-driven, algorithm-independent qualitative validation that complements the direct compositional validation described above. The recovered EEMs from one example pixel from each class are exposed in the **Fig 3**. It can be observed that the pure Hlina **(1)** resulted in higher emission around λ_{exc} ~ 365 nm, while the pure Ha **(7)** dots' emission is concentrated at λ_{exc} ~ 325 nm. The mixture dots EEMs are composed by a mixture of both signals.

5. DESIGN CONSIDERATIONS AND LIMITATIONS

During the design, engineering, and iterative fabrication of this phantom, we conducted several experiments to evaluate physical limitations and avoid measurement artifacts:

- *Dye Selection*: In our setup, EEM-HSI datasets were acquired across $\lambda_{exc}/\lambda_{em}$ ranges of 310-415 nm and 420-720 nm, respectively. For benchmarking systems operating in other spectral windows, alternative fluorophore pairs (such as riboflavin or fluorescein) or inorganic fluorescent standards can be implemented to enhance long-term photostability.
- *Solvent and pH Optimization*: Solvent selection requires ensuring chemical stability, high fluorescence quantum yield, and negligible background absorbance within the

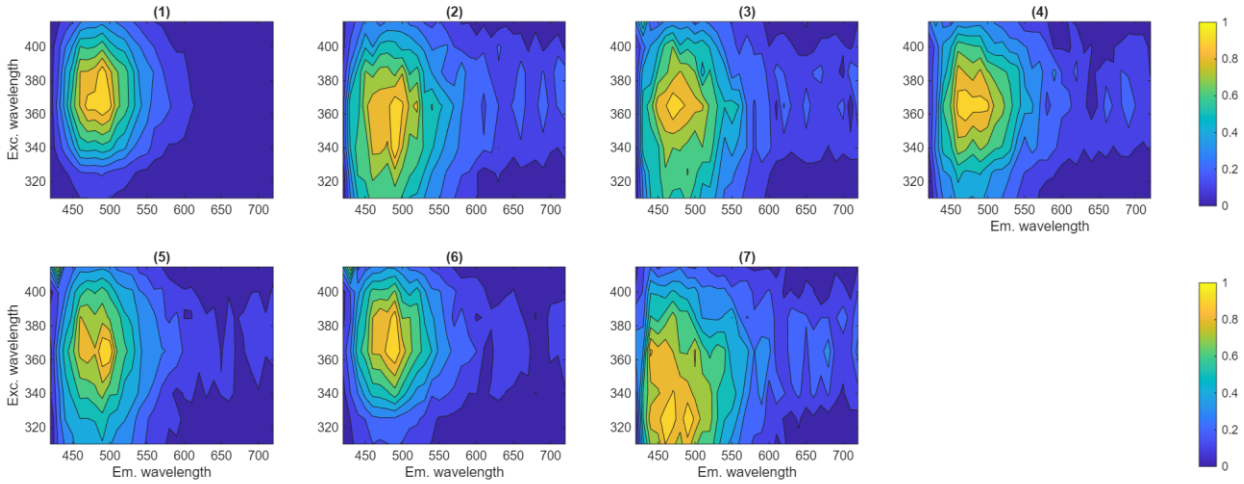


Figure 3. EEMs obtained from representative pixels belonging to each class in the phantom. Numbers indicate the dot class as denoted in **Fig. 1**.

target spectral window. In our initial solvent optimization experiments, we tested stock solutions across a range of pH values. We found that off-target pH levels either quenched dye fluorescence or accelerated chemical degradation, confirming that buffer conditions must be validated for the selected fluorophores prior to phantom casting.

- *Solid Matrix Selection and Coffee-Ring Effects*: We opted for a solid polymer matrix over liquid mixtures to eliminate handling shortcomings such as solvent evaporation, microbial contamination, temperature sensitivity, and long-term signal degradation. In testing candidate solid matrices, we evaluated matrix background absorption, dye-polymer chemical interactions, and spatial drying dynamics—in order to minimize the "coffee-ring" effect and to ensure homogeneous fluorophore distribution across each dot. For instance, in our trial formulations using polyvinyl acetate (PVAc), the resulting dots dried into highly scattering, opaque structures appearing white to the naked eye, which introduced severe attenuation artifacts into fluorescence measurements. Switching to PVA successfully resolved these issues, yielding highly transparent, non-scattering solid dots with uniform spatial emission.

6. DISCUSSION

The phantom described here is deliberately narrow in scope — two dyes, seven mixture classes, a single spatial layout — by design. Its purpose is to provide an unambiguous, validated ground truth for the specific spectral regime (*Scenario C*) that EEM-HSI is uniquely positioned to resolve, rather than to serve as a general-purpose multi-analyte target. This narrowness is what makes the validation in Section 4 tractable and the resulting benchmark trustworthy. Extensions of this design — additional dye pairs spanning *Scenarios A* and *B*, finer mixture-ratio sampling, or three-component mixtures — are natural directions for follow-up phantoms but are outside the scope of the present work.

Future work will focus on the detailed description and validation of each dot composition by standard analytical chemistry techniques, as solid-state EEMs obtention using a benchtop spectrofluorometer. This complete characterization will allow us to release the EEM-HSI datasets together with the characterization data in an open-source repository such as *Zenodo*, so it can be used as a reference for further work on computational analysis methods development.

7. CONCLUSION

We presented the design, fabrication, and compositional validation of a two-dye fluorescence phantom purpose-built to benchmark EEM-HSI unmixing in the excitation-discriminating, emission-overlapping regime (*Scenario C*). The phantom's seven-class mixture series, their disposition on glass, and validated ground truth are intended as a reusable resource. It can be used for evaluating instrumental artifacts and analytical processing as chemometric unmixing methods (MCR-ALS, PARAFAC, and others) on EEM-HSI data, independent of any single analysis performed on it.

8. ACKNOWLEDGEMENTS

This work was supported by the European Union ERA CHAIR award (NAS-SAR 101087403), the United States R44 HL120511, and the Republic of Armenia HESC (24PostDoc/2-2G002) grant. We thank to Dr. Franco M. Cabrerizo, who kindly provided us with the β-carboline alkaloids pure solids.

9. REFERENCES

[1] N. Chilingaryan, F. Villarruel, T. Soghomonyan, V. Yeghiazaryan, and N. Sarvazyan, "4D hyperspectral imaging for intraoperative tissue classification," in *Proc. SPIE 13410, Medical Imaging 2025: Clinical and Biomedical Imaging*, 2025, pp. 1–6. doi: 10.1117/12.3047177.

[2] N. Chilingaryan, A. Gasparyan, and N. Sarvazyan, "MULTIEXCITATION HYPERSPECTRAL IMAGING TOWARD IMPROVED LICHEN IDENTIFICATION," in *WHISPERS*, 2025, pp. 3–7.

[3] O. Katz, T. Ferguson, E. Abbey, S. J. Klose, C. Prüfert, and H. P. Loock, "Fluorescence Excitation-Emission-Matrix Imaging," *Anal. Chem.*, vol. 95, no. 34, pp. 12631–12639, 2023, doi: 10.1021/acs.analchem.3c00217.

[4] T. Ferguson and H. Loock, "Rapid Fluorescence EEM spectra acquisition using super-cycle Hadamard-Transform Multiplexing," *Anal. Chem.*, vol. 95, no. 34, pp. 12691–12700, 2023, doi: 10.1021/acs.analchem.3c01245.

[5] M. Balon, J. Hidalgo, P. Guardado, M. A. Muñoz, and C. Carmona, "Acid-Base and Spectral Properties of b-Carbolines. Part 2. Dehydro and Fully Aromatic b-Carbolines," *J. Chem. Soc. Perkin Trans*, vol. 2, pp. 99–104, 1993, doi: 10.1039/P29930000099.

[6] F. Villarruel *et al.*, "Light-induced full aromatization and hydroxylation of 7-methoxy-1-methyl-3,4-dihydro-2H-pyrido[3,4-b]indole alkaloid: Oxygen partial pressure as a key modulator of the photoproducts distribution," *J. Photochem. Photobiol. B Biol.*, vol. 199, no. August, p. 111600, 2019, doi: 10.1016/j.jphotobiol.2019.111600.

[7] M. M. Gonzalez, J. Arnbjerg, M. P. Denofrio, R. Erra-Balsells, P. R. Ogilby, and F. M. Cabrerizo, "One- and two-photon excitation of β-carbolines in aqueous solution: ph-dependent spectroscopy, photochemistry, and photophysics," *J. Phys. Chem. A*, vol. 113, no. 24, pp. 6648–6656, 2009, doi: 10.1021/jp902105x.

[8] T. Volkova, O. Simonova, and G. Perlovich, "Bridging the Knowledge Gap in Harmaline's Pharmacological Properties : A Focus on Thermodynamics and Kinetics," pp. 1–13, 2026.

[9] A. P. Varela, M. G. Miguel, A. L. Macanita, H. D. Burrows, and R. S. Becker, "β -Carboline Photosensitizers . 3 . Studies on Ground and Excited State Partitioning in AOT/Water/Cyclohexane Microemulsions," *J. Phys. Chem*, vol. 99, pp. 16093–16100, 1995.